Equine and Comparative Exercise Physiology 1(2); 141–150 DOI: 10.1079/ECEP200415

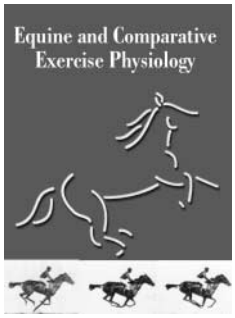

Quantification of three-dimensional skin displacement artefacts on the equine tibia and third metatarsus

Joel L Lanovaz[1,*], Siriporn Khumsap[2] and Hilary M Clayton[3]

[1]Department of Mechanical Engineering, McLaughlin Hall, Queen's University, 130 Stuart Street, Kingston, Ontario, Canada, K7L 3N6
[2]Faculty of Veterinary Medicine, Chiang Mai University, Thailand
[3]McPhail Equine Performance Center, Michigan State University, USA
*Corresponding author: lanovaz@me.queensu.ca

Submitted 26 June 2003: Accepted 27 January 2004 **Research Paper**

Abstract

Routine study of three-dimensional (3D) tarsal kinematics is hampered by errors due to the displacement of skin surface-tracking markers relative to the underlying bones. Reliable kinematics can be obtained with bone-fixed markers, but an accurate, non-invasive method would have more applications. Simultaneous kinematic data from skin-based and bone-fixed markers attached to the tibia and third metatarsus were collected from three trotting subjects. The motion of the skin-based markers was extracted relative to the underlying bone motion tracked using the bone-fixed markers. The 3D skin displacement patterns for the skin-based markers were parameterized using a truncated Fourier series model. These displacements were expressed in terms of the local coordinate system for each bone. Skin displacement artefacts were observed in all three axes of each bone segment, with the largest displacements occurring at the proximal tibia. The mean skin displacement amplitudes in the tibia were 6.7%, 3.2% and 10.5% of segment length, and for the third metatarsus were 2.6%, 1.4% and 3.8% of segment length, for the craniocaudal, mediolateral and longitudinal segment axes, respectively. Skin displacement patterns could be expressed concisely using the Fourier series model. Displacements were also consistent between subjects, which should allow them to be used as a basis for developing a correction procedure for 3D tarsal joint kinematics.

Keywords: tarsus; joints; kinematics; Fourier series; modelling

Introduction

The tarsal joint is one of the primary sites of lameness in the equine hind limb[1–3] and its basic kinematic parameters have been correlated with performance in sport horses[4]. Several studies have reported planar, two-dimensional (2D), equine tarsal joint motion[5–8], but only a few studies have examined three-dimensional (3D) equine tarsal kinematics either *in vitro*[9] or *in vivo*[10].

When skin surface markers are used to track segmental motion, 3D kinematics calculated from these markers is especially sensitive to skin motion artefacts. Relative displacements between skin and bone at some sites over the equine tibia have a range of motion of over 80 mm during a stride at the trot[11]. Marker cluster design and placement can reduce some errors[12], but actual underlying bone motion is still difficult to reproduce[13]. This is true even when utilizing a redundant marker set and a least-squares estimator of the transformation data[14].

Kinematic data collected using bone-fixed markers have been used to describe the true *in vivo* kinematics of joints in human subjects[13,15,16] and in horses[10,11]. The use of bone-fixed markers is invasive and it is desirable to develop procedures that avoid the need for surgical intervention but still produce an acceptable degree of accuracy.

Algorithms to correct for skin displacement artefacts have been successfully developed for 2D kinematics in horses[11,17], and this procedure has been shown to

improve joint angular data over non-corrected kinematics. The feasibility of using 3D correction algorithms has not been investigated in equine subjects.

The first step in developing a correction procedure for skin displacement artefacts is to characterize the 3D motion of the skin relative to the bone. In this study, simultaneous kinematic data collected from the skin surface and bone-fixed markers from the tibia and third metatarsus of equine subjects were used to parameterize the general motion of skin marker sites relative to the underlying bone. These parameters will be used in developing a model of the skin motion and a correction procedure.

Methods

Subjects

The subjects were three sound Quarter Horses of similar mass (mean ± standard deviation (SD) 353 ± 27 kg) and size (mean ± SD height at withers 1.44 ± 0.03 m). The horses were judged to be free of obvious lameness during a clinical examination prior to the study. The protocol used for this investigation was approved by the university's ethical use committee.

Bone-based markers

A detailed explanation of the bone-fixed procedure has been presented elsewhere[10]. In summary, 4.75 mm diameter Steinmann pins were inserted percutaneously under general anaesthesia into the tibia and third metatarsus of the right hind limb of each of the subjects. The tibial pin was placed mid-laterally, at the level of the calcaneal tuberosity and the metatarsal pin was placed mid-laterally in the bone, midway along its length. A small incision was made in the skin at the site of each pin, which minimized the effect of the pin on the local skin displacement. A marker triad with 25 mm diameter, reflective spherical markers was rigidly attached to each pin during the data collection session. Analgesics were administered systemically and locally, and all subjects appeared pain-free and moved normally during data collection.

Skin-based markers

A set of six, 25 mm diameter, spherical reflective markers was attached at predetermined locations on the surface of the skin over the right tibia and the right metatarsus of each subject (Fig. 1). This was in addition to the bone-fixed marker triads. The distance between markers TIB-A and TIB-B served as the reference length for the tibia and the distance between markers MET-A and MET-B served as the reference length for the third metatarsus. The skin-based markers were distributed over the lateral aspect of each segment, since most studies track kinematic data from the lateral side. Skin marker locations were a sufficient distance from the pin insertion sites so as to avoid any local skin displacement effects around the pins. The tibial markers were concentrated proximally in order to minimize visual merging with the bone pin marker triads.

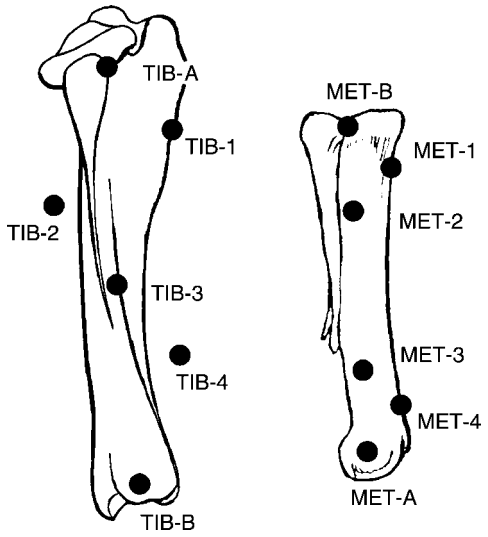

Fig. 1 Lateral view of the tibia (left) and third metatarsus (right) of a right limb showing the skin surface markers at the following locations: TIB-A, distal site of attachment of the lateral collateral femoro-tibial ligament; TIB-1, 1/6 of the segment length distal to TIB-A and over the tibial crest; TIB-2, 1/6 of the segment length proximally from TIB-3 and approximately 1/6 of the segment length caudal to the TIB-A/TIB-B line; TIB-3, midway along the line between TIB-A and TIB-B; TIB-4, 1/6 of the segment length distally from TIB-3 and about 1/6 of the segment length cranial to the line between TIB-A and TIB- B; TIB-B, over the lateral malleolus of the tibia; MET-B, dorsal edge of the head of the fourth metatarsal bone; MET-1, dorsal aspect of the bone midway between MET-B and MET-2; MET-2, 1/4 of the segment length distally from MET-B; MET-3, 1/4 of the segment length proximally from MET-A; MET-4, dorsal aspect of the bone midway between MET-A and MET-3; MET-A, metatarsal attachment of the lateral collateral ligament of the metatarsophalangeal joint. Not shown are the markers TIB-C and MET-C which are used during the standing reference pose and are placed on the medial side of the limb, opposite to TIB- B and MET-B, respectively

Bone coordinate systems

To define local bone-based coordinate systems (BCSs), all subjects were placed in a normal standing position and an additional reflective marker was placed over the medial malleolus of the tibia (TIB-C) and the dorsal edge of the head of second metatarsal bone (MET-C). These markers were removed before collecting data at the trot.

A right-handed coordinate system was developed for the tibia by first defining the flexion/extension axis as the unit vector running from TIB-B to TIB-C. The adduction/abduction axis of the tibia was defined as a unit vector pointing cranially and perpendicular to the plane formed by the flexion/extension axis and the vector running from TIB-B to TIB-A. Finally, the

internal/external rotation axis of the tibia was defined as a unit vector pointing proximally along the long axis of the bone and perpendicular to the plane formed by the flexion/extension and adduction/abduction axes. The origin of the tibial BCS was embedded in the bone midway between TIB-B and TIB-C.

The third metatarsal BCS was defined in a similar manner to the tibial system, with the flexion/extension axis defined as a unit vector running from MET-B to MET-C. The adduction/abduction axis was defined as a unit vector pointing cranially and perpendicular to the plane formed by the flexion/extension axis and the vector running from MET-B to MET-A. The internal/external rotation axis was defined as pointing proximally and perpendicular to the other two axes, forming a right-handed coordinate system. The origin of the third metatarsal BCS was embedded in the bone midway between MET-B and MET-C.

Data collection

All subjects were led in hand at the trot along a 40 m, rubber-covered concrete runway. Three-dimensional kinematic data were collected using a six-camera analysis system (ExpertVision RealTime; Motion Analysis Corporation, Santa Rosa, CA) recording at 120 frames s^{-1}. A volume measuring 5 m by 2 m by 3 m was calibrated and the mean error in measuring a known length within the volume was 0.88 mm[10]. Each successful trial consisted of a single stride of the right hind limb, starting with stance. Data collected from a force platform (LG6-4-8000; AMTI, Watertown, MA) embedded in the runway were used to detect the onset and termination of the right hind stance. Termination of a right hind stride was determined by an automatic algorithm that matched terminal swing-phase kinematics to the kinematic pattern at the beginning of the previous stance phase. The kinematic data from the trot trials were optimally filtered using a Generalized Cross Validation (GCV) spline routine[18]. The bone-fixed triads and the skin-based markers were tracked simultaneously for each trial. Four strides from each horse were selected. Trials were selected to closely match forward velocities between subjects.

Reference kinematics

The 3D kinematics of the tibia and third metatarsus, as calculated by the motion of the bone-fixed triads, was defined as the 'true' reference kinematics of the bones. The orientation matrices and displacement vectors for the reference kinematics were calculated by relating the locations of the triads in their corresponding BCS with their global locations during each frame-of-motion datum using a singular-value decomposition method[19].

Quantification of skin displacement

The 3D movements of the skin-based markers in the global coordinate system were collected for the motion data. The data from each frame were transformed using the orientation matrices and displacement vectors calculated from the bone-fixed triads and expressed in terms of their corresponding BCS. The skin-based data from each subject were normalized to a percentage of the segment reference length calculated from the standing pose.

The data from the skin-based markers were parameterized by representing the data from each coordinate of each marker as a truncated Fourier series[11,20] given by

$$C(t) = p_0 + \sum_{k=1}^{n} p_k \cos\left(\frac{2\pi k t}{100}\right) + \sum_{k=1}^{n} q_k \sin\left(\frac{2\pi k t}{100}\right), \quad (1)$$

where *C(t)* is an *x*-, *y*- or *z*-coordinate of a skin-based marker, t is expressed as a percentage of cycle time, p_0 is the constant offset, p_k and q_k are Fourier series parameters and n is the number of harmonics used to describe the data.

To determine n for each coordinate, the pooled data from all 12 trials were fit to equation (1) using a standard linear least-squares method, with n ranging from 1 to 30. A GCV criterion method[21] was used to find the statistically optimal n for each coordinate of each marker and the Fourier parameters p_o, p_k, and q_k were then calculated. Model parameters were also calculated for each subject, using the optimum number of harmonics derived from the fit to the complete pool of trials[11].

To minimize the effects of any marker placement variation between subjects, the standing pose value of the coordinate (expressed as a percentage of segment length) was subtracted from the skin displacement prior to fitting the data to the Fourier series. The p_0 value in the model then became a mean offset from the standing pose. The standing pose value for the subject was added to the results from the Fourier model to obtain a final value.

As an estimate of the goodness-of-fit for the pooled data Fourier parameters, the root-mean-square (RMS) fit error between the model and the actual data was calculated for each coordinate of each marker. The RMS and peak-to-peak amplitudes of the skin displacement for each coordinate of each marker were calculated from the fitted Fourier parameters.

The accuracy of the kinematic data collection system in the configuration used for this study was characterized as an error of the order of 0.88 mm

when measuring a known length[10]. It was decided that any coordinate model having peak-to-peak amplitude that was smaller than two times this error level would be considered too small to detect and not used. Similarly, any p_0 values that were less than this threshold were also set to zero.

For comparison, skin displacements for the *x*-axis and *z*-axis of TIB-A, TIB-B, MET-B and MET-A were calculated based on published 2D models[11,17] using mean kinematics from the 12 trials of the current study. The axes from van Weeren *et al.*[11] were transformed to correspond with the conventions used in this investigation.

Results

Descriptive data from the subjects and the kinematic trials are given in Table 1.

The reconstructions of the skin displacements from the Fourier model are shown in Figs 2 and 3. The skin displacements based on the pooled data and on the data for each of the three subjects are given on the same graph to enable any variation between horses to be visualized. The data from the model are plotted without adding the standing pose value so that they can be compared at similar scales. The values for the Fourier model parameters from the pooled data for

Table 1 Descriptive data from the subjects and the mean descriptive data from the kinematic trials

Subject	Height at withers (m)	Mass (kg)	Tibia length (mm)	Third metatarsus length (mm)	Velocity ($m\,s^{-1}$)	Stride time (ms)	Stance percentage
1	1.44	323	357	259	2.68	688	36.8
2	1.41	361	329	230	2.66	702	40.2
3	1.47	375	360	262	2.63	742	39.7
Mean (SD)	1.44 (0.03)	353 (27)	349 (17)	250 (18)	2.66 (0.03)	711 (28)	38.9 (1.8)

SD – standard deviation.

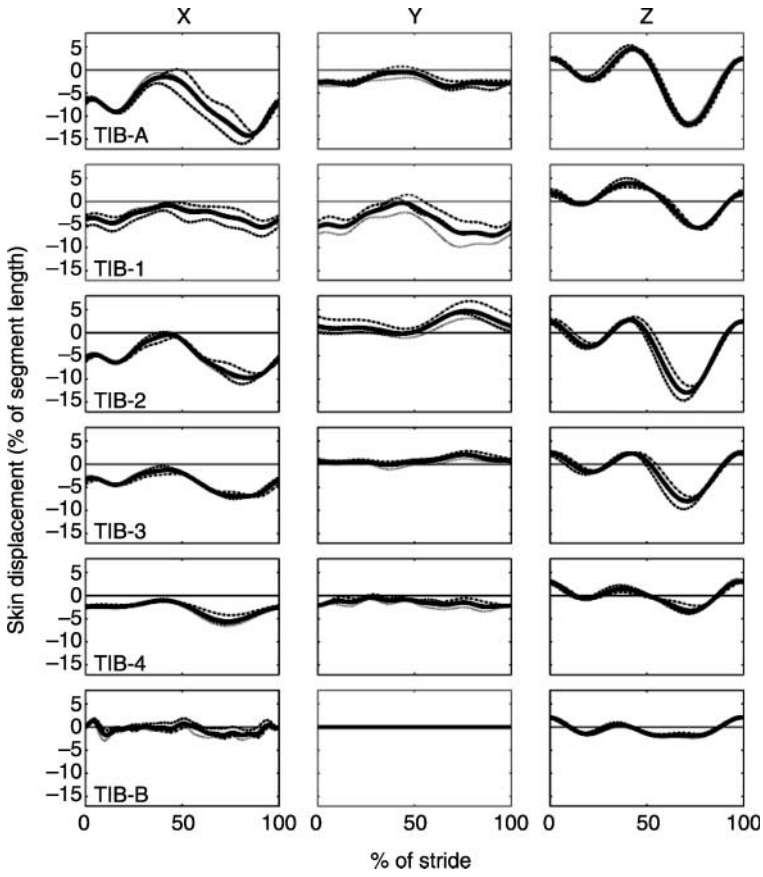

Fig. 2 Skin displacements for each coordinate of each tibial marker. The data are generated from the truncated Fourier series models. The dashed and dotted lines are from models fit to the three individual horses, while the thick solid line is from the model based on the pool of the 12 trials. The columns X, Y and Z represent the *x*-, *y*- and *z*-coordinate, respectively. Each row represents a marker, with the top row being TIB-A and the bottom row being TIB-B

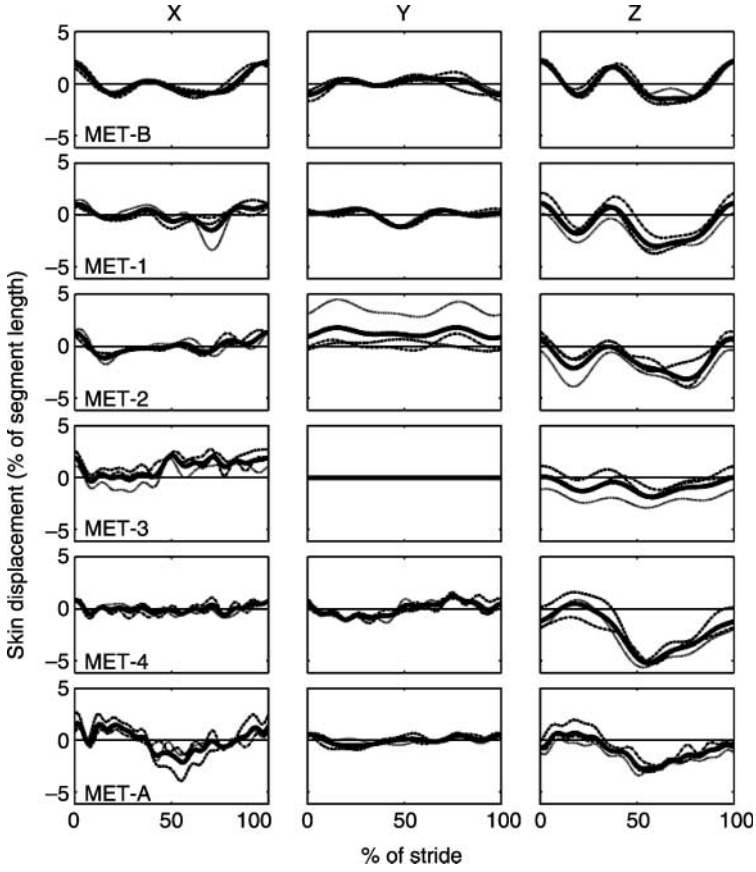

FIG. 3 Skin displacements for each coordinate of each third metatarsal marker. The data are generated from the truncated Fourier series models. The dashed and dotted lines are from models fit to the three individual horses, while the thick solid line is from the model based on the pool of the 12 trials. The columns X, Y and Z represent the *x*-, *y*- and *z*-coordinate, respectively. Each row represents a marker, with the top row being MET-B and the bottom row being MET-A

the tibia markers are given in Tables 2 and 3, and the parameters for the metatarsal markers are given in Tables 4 and 5. The data are presented as a percentage of segment reference length. The mean values for the standing pose locations of the markers are given in Table 6.

The skin displacement patterns for the *x*-axis and *z*-axis of the tibial markers showed similar trends, with higher amplitudes at the proximal locations. The *y*-axis of the tibial markers showed little movement except for TIB-1 and TIB-2, which were located furthest from the reference line of the segment.

Table 2 Fourier model parameters for the *x*-, *y*- and *z*-coordinates of the three proximal tibia skin markers. Parameter values are expressed as a percentage of segment length

	TIB-A			TIB-1			TIB-2		
	X	Y	Z	X	Y	Z[a]	X	Y	Z
p_0	−7.427	−2.249	−1.972	−3.137	−4.268	−0.443	−5.328	1.853	−2.970
p_1	−3.247	−0.920	0.053	−1.710	−2.430	−1.194	−2.528	0.636	1.234
q_1	3.554	0.706	4.963	0.469	1.920	2.888	2.793	−1.830	4.845
p_2	2.039	0.399	4.448	0.082	0.720	2.389	1.395	−1.015	4.193
q_2	−0.331	−0.589	−2.185	−0.103	−0.378	−0.760	−0.449	−0.002	−2.705
p_3	1.236	−0.102		0.395	0.079	0.653	0.567		
q_3	0.527	0.129		0.351	0.124	−0.386	0.512		
p_4	0.608	0.116		0.178	0.182		0.374		
q_4	0.235	0.205		0.141	0.183		0.198		
p_5				0.204	0.177		−0.055		
q_5				0.284	0.277		0.219		

[a] p_0 value is below the detectable threshold.

Table 3 Fourier model parameters for the *x*-, *y*- and *z*-coordinates of the three distal tibia skin markers. Parameter values are expressed as a percentage of segment length

	TIB-3			TIB-4			TIB-B		
	X	Y	Z	X	Y	Z[a]	X	Y[a,b]	Z
p_0	−4.054	0.815	−1.384	−3.000	−1.458	0.074	−0.513	0.177	−0.519
p_1	−1.183	0.163	0.917	−0.308	−0.374	0.902	−0.122	0.056	0.975
q_1	2.065	−0.737	3.033	1.751	0.591	1.312	0.572	0.037	0.545
p_2	1.105	−0.307	3.005	0.819	−0.198	1.597	0.660		0.869
q_2	−0.280	0.067	−1.729	−0.413	0.004	−0.990	−0.100		−0.712
p_3	0.368	−0.098			−0.036	0.539	0.191		0.751
q_3	0.186	0.046			0.147	−0.267	−0.214		0.071
p_4	0.292	0.179			0.159		0.456		
q_4	0.225	−0.039			0.087		0.138		
p_5	0.054				−0.108		0.086		
q_5	0.116				0.035		−0.063		
p_6					−0.133		0.049		
q_6					−0.101		0.160		
p_7							−0.148		
q_7							0.150		
p_8							−0.129		
q_8							0.160		
p_9							−0.217		
q_9							0.065		
p_{10}							−0.137		
q_{10}							0.049		
p_{11}							−0.185		
q_{11}							0.071		

[a] p_0 value is below the detectable threshold. [b] Peak-to-peak amplitude is below the detectable threshold.

Table 4 Fourier model parameters for the *x*-, *y*- and *z*-coordinates of the three proximal metatarsal skin markers. Parameter values are expressed as a percentage of segment length

	MET-B			MET-1			MET-2		
	X[a]	Y[a]	Z[a]	X[a]	Y[a]	Z	X[a]	Y	Z
p_0	−0.344	−0.053	−0.586	−0.629	−0.537	−1.069	−0.017	1.325	−1.350
p_1	0.818	−0.468	0.541	0.510	0.390	0.768	0.269	0.073	0.472
q_1	0.027	−0.112	0.787	0.232	0.022	1.000	−0.346	0.022	0.797
p_2	0.753	−0.360	0.951	0.379	−0.447	0.733	0.426	−0.304	0.845
q_2	−0.577	0.212	−0.765	−0.470	0.130	−0.907	−0.330	0.115	−0.673
p_3	0.378	−0.259	0.660	0.079	0.277	0.708	0.192	−0.173	0.666
q_3	0.020	−0.053	0.317	−0.067	−0.100	0.325	−0.050	0.205	−0.164
p_4				−0.178			0.267		
q_4				0.273			0.250		
p_5				0.218			0.192		
q_5				0.084			0.002		

[a] p_0 value is below the detectable threshold.

The *y*-coordinate artefact of the TIB-B position showed peak-to-peak and p_0 values below the detectable threshold and therefore no correction was applied to that coordinate. On the third metatarsus, the displacement patterns for the *x*-axis and *z*-axis of the markers had similar amplitudes and trends during the swing phase, but during the stance phase the displacement at the proximal end of the segment was in the opposite direction to that of the distal end. The *y*-axis displacements of the third metatarsal segment markers had small amplitudes and higher variability between sites and subjects, with the MET-3 *y*-axis artefact having a peak-to-peak amplitude below detectable levels. Overall, the tibial markers underwent much larger displacements than those on the third metatarsus.

The optimal number of harmonics, the p_0 value, the RMS fit error of the pooled model to the actual skin displacement, and the RMS and peak-to-peak amplitudes of the skin displacement models are summarized in Table 7. The RMS amplitude of the skin displacement for the tibial markers ranged from 0.1 to 7.0% of the segment length, with the average being 2.9% of segment length. This corresponds to an approximate displacement of 10 mm. The largest peak-to-peak amplitude of skin displacement in the tibial markers was for the *z*-axis of marker TIB-A, which showed a range of motion of 16.4% of segment length or approximately 57 mm. The tibial p_0 values averaged about 2% of segment length (approximately 7 mm), with the TIB-1 and TIB-4 *z*-coordinate p_0 values being

Table 5 Fourier model parameters for the *x*-, *y*- and *z*-coordinates of the three distal metatarsal skin markers. Parameter values are expressed as a percentage of segment length

	MET-3			MET-4			MET-A		
	X	Y[a,b]	Z	X[a]	Y[a]	Z	X[a]	Y[a]	Z
p_0	0.968	0.013	−0.881	0.654	0.691	−2.197	−0.266	0.649	−0.964
p_1	−0.057	0.034	0.492	0.231	0.041	1.598	1.185	0.131	0.982
q_1	−0.862	0.260	0.181	−0.031	−0.822	1.932	0.616	−0.309	1.073
p_2	0.356	−0.053	0.196	0.068	0.000	−0.585	−0.384	0.196	−0.353
q_2	−0.085	−0.011	−0.307	−0.036	0.031	−0.144	−0.056	−0.047	0.000
p_3	0.006	0.022	0.230	0.175	−0.036	0.154	0.195	0.011	−0.027
q_3	−0.142	0.153	0.306	−0.127	0.077	0.049	−0.217	0.125	0.130
p_4	0.280	−0.003		0.033	0.180	−0.161	0.040	0.130	−0.037
q_4	−0.173	0.089		−0.165	0.109	−0.158	−0.253	0.100	−0.126
p_5	−0.071			0.002	0.000		−0.037	0.081	−0.079
q_5	−0.059			−0.011	−0.040		−0.048	−0.011	0.059
p_6	0.296			0.155	0.037		0.184		−0.113
q_6	0.030			0.041	−0.013		0.002		−0.088
p_7	0.046			0.070	0.082		0.041		0.005
q_7	0.033			0.035	−0.003		0.064		0.001
p_8	0.135			0.053	0.178		0.168		−0.073
q_8	−0.083			−0.070	0.005		−0.052		−0.005
p_9	−0.055			−0.026			−0.003		0.020
q_9	0.118			0.133			0.229		−0.092
p_{10}	0.015			0.013			0.061		−0.025
q_{10}	0.125			0.116			0.173		−0.088
p_{11}							0.016		
q_{11}							0.099		
p_{12}							−0.089		
q_{12}							0.121		

[a] p_0 value is below the detectable threshold. [b] Peak-to-peak amplitude is below the detectable threshold.

Table 6 Mean (SD) marker locations from the standing poses. Data are expressed with respect to the local bone coordinate systems and are given as a percentage of segment length

Marker	X	Y	Z
TIB-A	0 (0)	−21 (2)	100 (0)
TIB-1	14 (3)	−6 (3)	87 (3)
TIB-2	−14 (2)	−23 (2)	72 (4)
TIB-3	−2 (2)	−22 (1)	52 (2)
TIB-4	12 (3)	−12 (0)	36 (6)
TIB-B	0 (0)	−17 (1)	0 (0)
MET-B	0 (0)	−18 (1)	0 (0)
MET-1	16 (2)	−9 (2)	−13 (1)
MET-2	−3 (2)	−13 (2)	−28 (2)
MET-3	−2 (2)	−13 (2)	−74 (2)
MET-4	14 (0)	−7 (4)	−88 (4)
MET-A	0 (0)	−19 (1)	−100 (0)

SD – standard deviation.

below detectable levels. For the third metatarsal segment, the RMS skin displacement amplitudes ranged from 0.3 to 2.6% with an average value of 1.6%, corresponding to an approximate value of 4 mm. The largest peak-to-peak amplitude of skin displacement in the third metatarsal markers was 5.7% of the segment length (approximately 14 mm), seen in the *z*-axis of marker MET-4. The p_0 values for the third metatarsus were relatively low (mean $<0.5\%$) with many below the detectable threshold (Tables 4 and 5).

The average number of harmonics required to model the skin displacements was between 3 and 4 for the tibia and between 5 and 6 for the third metatarsus. The pooled trial Fourier model showed a good fit to the actual skin data, with most values for the RMS fit error being well below the peak-to-peak amplitude of the displacement itself (Table 7). The largest RMS fit error for the tibial markers was the *x*-axis of TIB-A at 2.1% of segment length. For the metatarsus, the largest RMS fit error was 2.1% of segment length on the *y*-axis of MET-1.

The skin displacements for the *x*-axis and *z*-axis of TIB-A, TIB-B, MET-B and MET-A calculated from 2D models given by van Weeren *et al.*[11] were plotted against the current data (Fig. 4). In general, the 2D study tended to estimate a larger range of skin displacement than the current study.

Discussion

The periodic nature of the skin displacement lends itself to being modelled with a truncated Fourier series. The general displacement patterns were reproducible within and between subjects and this was reflected in the low fit errors. It has been shown that 2D skin displacement in the equine proximal limb is not highly correlated with adjacent joint flexion angles[11]. Visual inspection of the data from the current study shows that, with the exception of some of the *z*-coordinate data, the 3D displacement patterns are also not strongly correlated with published tarsal flexion angles. It may be that a complex relationship between the three angular

Table 7 Descriptive statistics from the modelled skin displacements for the *x*-, *y*- and *z*-coordinate for each skin surface marker. The order indicates the optimal number of harmonics in the Fourier model and the p_0 value is the mean offset from the standing pose location. RMS error is the difference between the actual displacement and the model. RMS amp and Peak amp are the RMS and peak-to-peak amplitudes of the skin displacement calculated using the model. All percentage values refer to percentage of the tibia or third metatarsus segment length

	X					Y					Z				
Marker	Order (*n*)	p_0 (%)	RMS error (%)	RMS amp (%)	Peak amp (%)	Order (*n*)	p_0 (%)	RMS error (%)	RMS amp (%)	Peak amp (%)	Order (*n*)	p_0 (%)	RMS error (%)	RMS amp (%)	Peak amp (%)
TIB-A	4	−7.4	2.1	5.4	12.7	4	−2.2	0.9	1.4	3.0	2	−2.0	1.1	7.0	16.4
TIB-1	5	−3.1	1.6	1.9	4.8	5	−4.3	1.8	3.2	7.1	3	−0.4	1.0	4.1	9.7
TIB-2	5	−5.3	1.2	4.1	9.4	2	1.9	1.4	2.2	4.9	2	−3.0	1.3	7.1	15.8
TIB-3	5	−4.1	0.8	2.7	5.7	4	0.8	0.6	0.8	2.2	2	−1.4	1.1	4.7	10.6
TIB-4	2	−3.0	0.7	2.0	4.5	6	−1.5	0.6	0.8	2.0	3	0.1	0.7	2.5	6.4
TIB-B	11	−0.5	0.8	1.2	3.2	1	0.2	0.6	0.1	0.1	3	−0.5	0.5	1.8	4.0
MET-B	3	−0.3	1.1	1.3	3.0	3	−0.1	1.0	0.7	1.6	3	−0.6	0.7	1.7	3.6
MET-1	5	−0.6	1.4	0.9	2.5	3	−0.5	2.1	0.7	1.7	3	−1.1	0.8	1.9	4.1
MET-2	5	0.0	1.3	0.8	2.5	3	1.3	1.9	0.4	1.0	3	−1.3	1.2	1.6	3.8
MET-3	10	1.0	0.8	1.1	2.5	4	0.0	0.9	0.3	0.7	3	−0.9	1.0	0.7	1.9
MET-4	10	0.7	0.8	0.5	1.4	8	0.7	1.2	0.9	2.3	4	−2.2	0.9	2.6	5.7
MET-A	12	−0.3	0.9	1.5	3.8	5	0.6	0.6	0.4	1.1	10	−1.0	0.6	1.5	3.5

RMS – root-mean-square.

FIG. 4 Comparison of skin displacement models for the proximal and distal ends of the tibia and third metatarsus. The solid lines are from the models for the TIB-A, TIB-B, MET-A and MET-B markers from the current study. The open dotted lines are from the models given in van Weeren *et al.*[11] for the corresponding locations. The first column is the displacement data for the *x*-axis and the second column is the displacement data for the *z*-axis. The data are given as a percentage of segment length

degrees of freedom and the skin displacement patterns does exist and might be modelled, but it can be argued that the Fourier series model presented here is a sufficient and practical approach.

The only previous equine skin displacement investigation[11] developed regression equations for four of the sites looked at in this study. Despite differences between that study and the current one in terms of the nature of the data (i.e. 2D vs. 3D) and differences in subject breeds and sizes, the data are quite comparable. Although van Weeren *et al.*[11] gave models for the *x*-axis displacements of both ends of the third metatarsus, their original data were within the systematic error range of their study and they deemed the models not useful for correction. This may explain the differences in those axes compared with the results presented here. The other difference between the two studies is an offset seen in the *x*-axis displacement data of the proximal tibia. Van Weeren *et al.*[11] assumed that the skin oscillates around the original marker position and therefore the p_0 value of their Fourier model was set to zero before fitting the data.

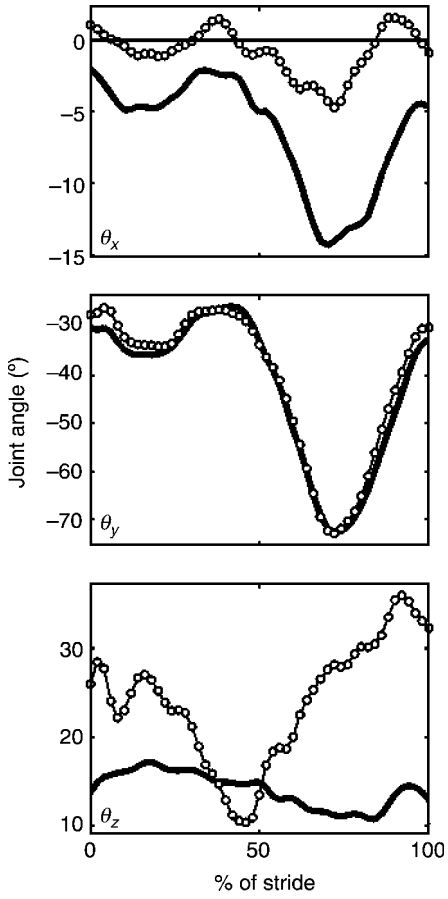

FIG. 5 Comparison of tarsal joint kinematics derived from bone-fixed and uncorrected skin-based markers. θ_x, θ_y and θ_z are the attitude vector angles corresponding to the adduction(+)/-abduction(−), flexion(−)/extension(+) and internal(+)/-external(−) rotation angles, respectively[10]. The solid lines are data from the bone-fixed markers while the open circles represent data from the skin-based markers. Data are from a single trial of one subject

The current study found that this assumption is probably valid for the third metatarsus and distal tibia, but is not true for the proximal tibia.

Significant *y*-axis (mediolateral) skin displacement artefacts were recorded in this study, which points to the fact that the 3D nature of the artefacts must be taken into account. To highlight this, 3D tarsal joint angle kinematics for a representative stride of a single subject is shown in Fig. 5. The kinematic data were calculated using a procedure described previously[10]. Data obtained from bone-fixed markers are compared with data from the skin-based markers. The flexion angle data are remarkably similar for the two marker sets, showing that little correction may be needed for that degree of freedom if 3D marker sets are utilized. However, kinematics obtained from the skin-based markers shows a large underestimation of the abduction angle and a completely improbable overestimation of the internal rotation angle.

It is clear that if skin-based markers are to be used to obtain 3D kinematics of the tarsal joint, some type of correction must be applied to account for displacement artefacts. A general correction procedure could be developed if the displacement patterns are consistent between subjects. Correction algorithms for human kinematics have been shown to be problematic due to inter-subject variation[14]. The data obtained in the current study are more promising as there appear to be repeatable patterns across subjects for most of the marker coordinates.

This study has quantified the 3D skin displacement patterns for redundant kinematic marker sets on the tibia and third metatarsus at the trot. The displacement patterns were successfully modelled as truncated Fourier series, expressed in local bone coordinates and scaled to segment length. The data from this investigation will be used to develop a correction procedure to reduce the effect of skin motion artefacts on the 3D kinematics of the tibia, third metatarsus and the tarsal joint itself.

Acknowledgements

This work was supported by the McPhail Endowment, College of Veterinary Medicine, Michigan State University. The authors would like thank Drs John Stick and Jennifer Brown for performing the surgical procedures, and Carissa Wickens and Sarah Fox for assistance during data collection. The authors would also like to thank Dr Ton van den Bogert for providing additional information regarding the previously published 2D correction procedures.

References

1 Gabel AA (1983). Prevention, diagnosis and treatment of inflammation of the distal hock. *Proceedings of the 28th Annual Convention of the American Association of Equine Practitioners, Manhattan, NY*, pp. 287–298.

2 Winter D, Bruns E, Glodek P and Hertsch B (1996). Genetic disposition of bone diseases in sport horses. *Zuchtungskunde* **68**: 92–108.

3 Gough M and Munroe G (1998). Decision making in the diagnosis and management of bone spavin in horses. *In Practice* **20**: 252–259.

4 Holmström M, Fredricson I and Drevemo S (1995). Biokinematic effects of collection on the trotting gaits in the elite dressage horse. *Equine Veterinary Journal* **27**: 281–287.

5 Kobluk CN, Schnurr D, Horney FD, Hearn TC, Summer-Smith G, Willoughby RA *et al.* (1989). Use of high speed cinematography and computer generated gait diagrams for the study of equine hind limb kinematics. *Equine Veterinary Journal* **21**: 48–58.

6 Holmström M, Fredricson I and Drevemo S (1994). Biokinematic analysis of the Swedish Warmblood riding horse at trot. *Equine Veterinary Journal* **26**: 235–240.

7 Back W, Schamhardt HC, Savelberg HHCM, van den Bogert AJ, Bruin G, Hartman W *et al.* (1995). How the horse

moves: 2. Significance of graphical representations of equine hind limb kinematics. *Equine Veterinary Journal* **27**: 39–45.
8 Hodson EF, Clayton HM and Lanovaz JL (2001). The hind limb in walking horses: 1. Kinematics and ground reaction forces. *Equine Veterinary Journal* **33**: 38–43.
9 Schamhardt HC, Hartman W and De Lange A (1984). Kinematics of the equine tarsus. *Abstracts of the XV Congress of the European Association of Veterinary Anatomists, Utrecht, The Netherlands*, pp. 178–179.
10 Lanovaz JL, Khumsap S, Clayton HM, Stick JA and Brown J (2002). Three dimensional kinematics of the tarsal joint at the trot. *Equine Veterinary Journal Supplement* **34**: 308–313.
11 Van Weeren PR, van den Bogert AJ and Barneveld A (1992). Correction models for skin displacement in equine kinematic gait analysis. *Journal of Equine Veterinary Science* **12**: 178–192.
12 Cappozzo A, Cappello A, Della Croce U and Pensalfini F (1997). Surface-marker cluster design criteria for 3-D bone movement reconstruction. *IEEE Transactions on Biomedical Engineering* **44**: 1165–1174.
13 Cappozzo A, Catani F, Leardini A, Benedetti MG and Della Croce U (1996). Position and orientation in space of bones during movement: experimental artifacts. *Clinical Biomechanics* **11**: 90–100.
14 Reinschmidt C, van den Bogert AJ, Nigg BM, Lundberg A and Murphy N (1997). Effect of skin movement on the analysis of skeletal knee joint motion during running. *Journal of Biomechanics* **30**: 729–732.
15 Lafortune MA, Cavanagh PR, Sommer HJ III and Kalenak A (1992). Three-dimensional kinematics of the human knee during walking. *Journal of Biomechanics* **25**: 347–357.
16 Reinschmidt C, van den Bogert AJ, Murphy N, Lundberg A and Nigg BM (1997). Tibiocalcaneal motion during running – measured with external and bone markers. *Clinical Biomechanics* **12**: 8–16.
17 Van den Bogert AJ, van Weeren PR and Schamhardt HC (1990). Correction for skin displacement errors in movement analysis of the horse. *Journal of Biomechanics* **23**: 97–101.
18 Woltring HJ (1986). A FORTRAN package for generalized, cross-validatory spline smoothing and differentiation. *Advances in Engineering Software* **8**: 104–113.
19 Söderkvist I and Wedin P (1993). Determining the movements of the skeleton using well-configured markers. *Journal of Biomechanics* **26**: 1473–1477.
20 Cappozzo A, Leo T and Pedotti A (1975). A general computing method for the analysis of human locomotion. *Journal of Biomechanics* **8**: 307–320.
21 Woltring HJ (1990). Model and measurement error influences in data processing. *Biomechanics of Human Movement: Applications in Rehabilitation, Sports and Ergonomics*, Worthington, OH: Bertec Corporation, pp. 203–237.